Mesoscopic supercurrent transistor controlled by nonequilibrium cooling

F. Giazotto,[1,*] T. T. Heikkilä,[2] F. Taddei,[1] Rosario Fazio,[1] J. P. Pekola,[2] and F. Beltram[1]

[1] *NEST-INFM & Scuola Normale Superiore, I-56126 Pisa, Italy*

[2] *Low Temperature Laboratory, Helsinki University of Technology, P.O. Box 2200, FIN-02015 HUT, Finland*

The distinctive quasiparticle distribution existing under nonequilibrium in a superconductor-insulator-normal metal-insulator-superconductor (SINIS) mesoscopic line is proposed as a novel tool to control the supercurrent intensity in a long Josephson weak link. We present a description of this system in the framework of the diffusive-limit quasiclassical Green-function theory and take into account the effects of inelastic scattering with arbitrary strength. Supercurrent enhancement and suppression, including a marked transition to a π-junction are striking features leading to a fully tunable structure. The role of the degree of nonequilibrium, temperature, and materials choice as well as features like noise, switching time, and current and power gain are also addressed.

PACS numbers: 74.50.+r, 73.23.-b, 74.40.+k

I. INTRODUCTION

Nonequilibrium effects in mesoscopic superconducting circuits have been receiving a rekindled attention during the last few years [1]. The art of controlling Josephson coupling in superconductor-normal metal-superconductor (SNS) weak links is at present in the spotlight: a recent breakthrough in mesoscopic superconductivity is indeed represented by the SNS transistor, where supercurrent suppression as well as its sign reversal (π-transition) were demonstrated [2, 3, 4, 5, 6]. This was achieved by driving the quasiparticle distribution in the weak link far from equilibrium [7, 8, 9] through external voltage terminals, *viz.* normal reservoirs. Such a behavior relies on the two-step shape of the quasiparticle nonequilibrium distribution, typical of diffusive mesoscopic wires and experimentally observed by Pothier and coworkers [10].

The purpose of this paper is to demonstrate that it is possible to tailor the quasiparticle distribution through *superconductivity-induced* nonequilibrium in order to implement a unique class of superconducting transistors [11]. This can be achieved when mesoscopic control lines are connected to superconducting reservoirs through tunnel barriers (I), realizing a SINIS channel. The peculiar quasiparticle distribution in the N region, originating from biasing the S terminals, allows one to access several regimes, from supercurrent enhancement with respect to equilibrium to a large amplitude of the π-transition passing through a steep supercurrent suppression. These features are accompanied by a large current gain (up to some 10^5 in the region of larger input impedance) and reduced dissipation. The ultimate operating frequencies available open the way to the exploitation of this scheme for the implementation of ultrafast cryogenic current and/or power amplifiers.

The paper is organized as follows. In Sec. II we introduce diffusive-limit quasiclassical Green-function theory that is employed to describe the supercurrent in the proposed structure. In particular, we show how to exploit superconductivity-induced nonequilibrium in order to control the Josephson current. In Sec. III we address the role of inelastic scattering in the structure by solving the kinetic equation for the SINIS control line, and we describe how the strength of such scattering affects the observable supercurrent. The critical current dependence on the length of the weak link is analyzed in Sec. IV where the relevance of *long* junctions is pointed out. In Sec. V we consider the effect of the additional control terminals on the observable supercurrent while Sec. VI is devoted to the analysis of the supercurrent harmonics. In Sec. VII we address the role of materials combination in determining the performance of the structure. In particular, issues like power dissipation and noise power are discussed. The achievable current and power gain as well as the maximum attainable transistor operating frequency are discussed in Sec. VIII. Finally, Sec. IX summarizes the main results.

II. TRANSISTOR OUTPUT CHARACTERISTIC

The investigated mesoscopic structure (see Fig. 1) consists of a long diffusive weak link of length L_J much larger than the superconducting coherence length (ξ_0) oriented along the x direction. This defines the SNS junction of cross-section A_J. The superconducting terminals belonging to the SNS junction, labelled S_J (3 and 4), are kept at zero potential in the analysis of the supercurrent (transistor operation may take place in the dissipative regime at a finite voltage). The SINIS control line is oriented along the y direction and consists of a normal wire, of length L_C and cross-section A_C, connected through identical tunnel junctions of resistance $\mathcal{R}_T$ to two superconducting reservoirs S_C (1 and 2), biased at opposite voltages $\pm V_C/2$. The superconducting gaps of S_J and S_C (Δ_J and Δ_C) are in general different in order to optimize the structure characteristics.

The supercurrent I_J flowing across the SNS junction

*Electronic address: giazotto@sns.it

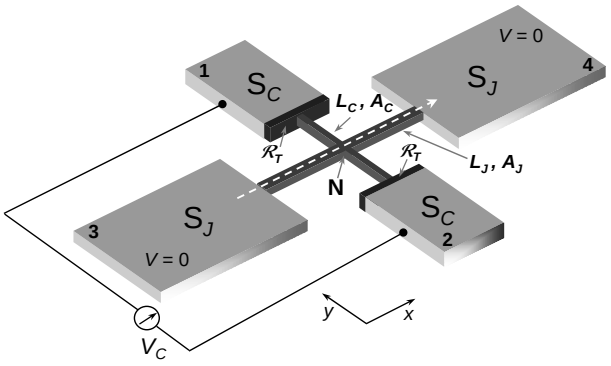

FIG. 1: Scheme of the Josephson transistor. The supercurrent I_J (along the white dashed line) is tuned by applying a bias V_C across the SINIS symmetric line connected to the center of the weak link. The superconducting gaps Δ_J and Δ_C are, in general, different, and all normal wires are assumed quasi-one-dimensional, i.e., their width is much smaller than their length.

is given by [8, 9]

$$I_J(V_C) = \frac{\sigma A_J}{eL_J}\int_0^\infty dE\,[f(-E;V_C) - f(E;V_C)]\mathrm{Im}[j_E], \tag{1}$$

and depends on the quasiparticle distribution function $f(E)$ in N. In Eq. (1), σ is the normal-state conductivity which determines the normal-state resistance of the junction according to $R_N = L_J/\sigma A_J$. As shown below, the distribution function f is determined by the SINIS control line and reduces to the equilibrium Fermi distribution when $V_C = 0$.

The energy-dependent spectral supercurrent, [12, 13] $\mathrm{Im}[j_E]$, can be calculated by solving the Usadel equations [14]. Following the parametrization of the Green functions given in Ref. 12, these equations in the N region can be written as

$$j_E = -\sinh^2(\theta)\partial_x\chi, \qquad \partial_x j_E = 0, \tag{2}$$

$$\hbar D\partial_x^2\theta + 2iE\sinh\theta - \frac{\hbar D}{2}(\partial_x\chi)^2\sinh(2\theta) = 0, \tag{3}$$

where $D = \frac{1}{3}v_F\ell_m$ is the diffusion coefficient, v_F is the Fermi velocity, ℓ_m is the mean free path and E is the energy relative to the chemical potential in S_J. $\theta(x,E)$ and $\chi(x,E)$ are in general complex functions. For perfectly transmissive contacts, the boundary conditions at the S_JN interfaces reduce to $\theta = \mathrm{arctanh}(\Delta_J/E)$ and $\chi = \pm\phi/2$ in the reservoirs S_J, where ϕ is the phase difference between the superconductors. The presence of the control wires on the spectral supercurrent can be taken into account explicitly including two additional probes and imposing boundary conditions at the S_CN interfaces as in Ref. [13]. In the present case such boundary conditions take the form $\partial_x\theta = 0$ to describe large tunnel barriers of resistance $\mathcal{R}_T$. The large $\mathcal{R}_T$ allows us to neglect the tiny oscillating supercurrents flowing between the superconductors S_C. As discussed in Sec. V, the supercurrent I_J depends trivially on the control wire length L_C, namely it monotonically decreases, rapidly reaching an asymptotic value of, roughly, one half the zero-length value. This in turn allows us to make the following simplifications: as far as the spectral current is concerned, we shall assume $L_C/L_J \to 0$, aware of the fact that the effect of a finite L_C/L_J gives rise to a mere reduction of I_J. A similar discussion can be made on the dependence of the equilibrium supercurrent on A_C. As shown in Ref. [13], I_J is a monotonically decreasing function of A_C/A_J and, as far as spectral supercurrent is concerned, we assume $A_C/A_J \to 0$ throughout the paper (in fact, it is enough to assume either $L_C \ll L_J$ or $A_C \ll A_J$).

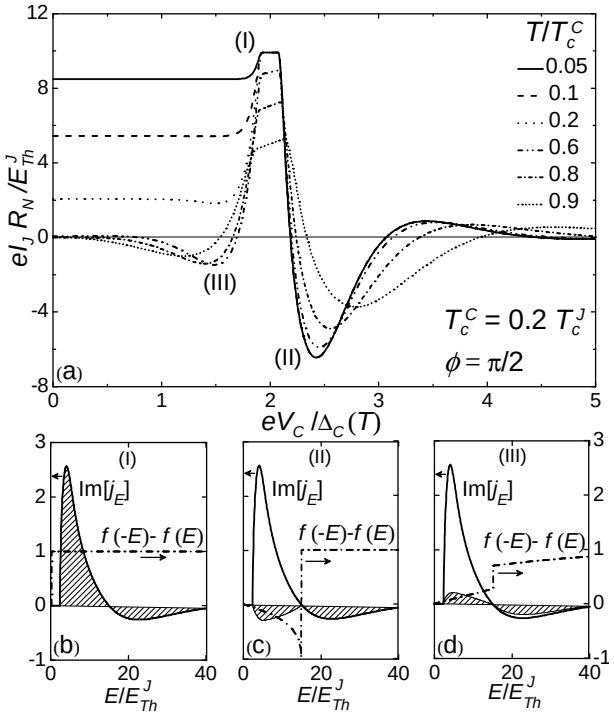

FIG. 2: (a) Supercurrent vs control voltage V_C at different temperatures (T) for $\phi = \pi/2$ and $T_c^C = 0.2\,T_c^J$ (see text). Bias regions labelled (I), (II) and (III) indicate supercurrent enhancement due to quasiparticle *cooling*, high-voltage π-state and low-voltage π-state in the high-temperature regime, respectively. These are qualitatively explained in (b), (c) and (d) where hatched areas represent the contribution to supercurrent arising in such bias ranges (see text). We assume throughout that supercurrent at $\phi = \pi/2$ yields values close enough to the critical current, an assumption that breaks down near the π-junction transition [6, 13] (see Sec. VI).

We must now determine the actual quasiparticle distribution f in the N region of the SINIS structure. This is controlled by voltage (V_C) and temperature, and by the amount of inelastic scattering in the control line. In the case of a short control wire with no inelastic interactions, the quasiparticle distribution, according to Ref. [15], is

given by

$$f(E,V_C)=\frac{\mathcal{N}_1\mathcal{F}_1+\mathcal{N}_2\mathcal{F}_2}{\mathcal{N}_1+\mathcal{N}_2}, \tag{4}$$

where $\mathcal{N}_{1,2}=\mathcal{N}_{S_C}(E\pm eV_C/2)$ and $\mathcal{F}_{1,2}=\mathcal{F}^0(E\pm eV_C/2)$. The former are the BCS density of states in the reservoirs S_C (labelled 1 and 2 in Fig. 1). $\mathcal{F}^0(E)$ is the Fermi function at lattice temperature T [17]. Note that expression (4) can also be found from the quasiclassical theory in the tunnelling limit [16]. In this case Eqs. (1) and (4) yield the dimensionless transistor output characteristics shown in Fig. 2(a), where we plot the supercurrent I_J versus control bias V_C at different temperatures. We assumed $\phi=\pi/2$, $T_c^C/T_c^J=0.2$, where $T_c^{C(J)}$ are the critical temperatures of the superconductors $S_{C(J)}$, and L_J such that $\Delta_J/E_{Th}^J=300$. We choose the limit of a long junction (i.e., $\Delta_J\gg E_{Th}^J$, where $E_{Th}^J=\hbar D/L_J^2$ is the Thouless energy of the SNS junction), since in this limit the supercurrent spectrum varies strongly with energy.

For all temperatures $T<T_c^C$, with increasing V_C, curves display a large supercurrent enhancement with respect to equilibrium at bias $V_C=2\,\Delta_C(T)/e=V_C^*(T)$ (region I in the figure). Further increase of the bias leads to a π-transition (region II) and finally to a decay for larger voltages [18]. This behavior is illustrated by Figs. 2(b,c,d) where the spectral supercurrent (solid line) is plotted together with $f(-E)-f(E)$ (dash-dotted line) for values of V_C and T corresponding to regions I, II and III, respectively. Hatched areas represent the integral of their product, i.e., the supercurrent I_J of Eq. (1). In particular, region I corresponds to the *cooling* regime where hot quasiparticles are extracted from the normal metal [15, 20]. The origin of the π-transition in region II is illustrated by Fig. 2(c), where the negative contribution to the integral is shown. We remark that the intensity of the supercurrent inversion is very significant. It reaches about 60% of the maximum value of I_J at $V_C\simeq V_C^*(T)$ in the whole temperature range, nearly doubling the π-state value of the supercurrent as compared to the case of an all-normal control channel [8, 9]. In the high-temperature regime ($T/T_c^C\geq 0.6$), when the equilibrium critical current is vanishing, the supercurrent first undergoes a low-bias π-transition (region III in the figure), then enters regions I and II. This recovery of the supercurrent from vanishingly small values at equilibrium is again a consequence of the peculiar shape of f (see Fig. 2(d)). Notably, the supercurrent enhancement around $V_C^*(T)$ remains pronounced even at the highest temperatures, so that I_J attains values largely exceeding 50% of the junction maximum supercurrent. This demonstrates the strong tunability of the supercurrent through nonequilibrium effects induced by the superconducting control lines. We remark that this is a unique feature stemming from the superconductivity-induced nonequilibrium population in the weak link.

III. ROLE OF INELASTIC SCATTERING

Since we do not want to confine our analysis only to the limit of control wires much shorter than the energy relaxation length, we need to evaluate the impact of inelastic scattering present in the N region on the supercurrent behavior [21]. As a matter of fact, the length L_C of the SINIS control line can be additionally varied to control the supercurrent by changing the effective strength of inelastic scattering in the N region. In general, the steady state distribution function at a given energy E is determined by an equation which accounts for the balancing of quasiparticle flow to and from the reservoirs with a collision term $\mathcal{I}$, describing energy relaxation processes. For $\mathcal{R}_T\gg R_C=L_C/\sigma A_C$, the distribution function $f(E)$ in the N region is essentially y-independent and we have

$$\frac{1}{e^2\mathcal{R}_T\Omega_C\nu_F}[\mathcal{N}_1(\mathcal{F}_1-f(E))+\mathcal{N}_2(\mathcal{F}_2-f(E))]+ \\ +\kappa\int d\omega d\varepsilon\,\omega^\alpha\mathcal{I}(\omega,\varepsilon,E)=0. \tag{5}$$

Here ν_F is the normal-metal density of states at the Fermi energy, Ω_C is the volume of the N region and $\mathcal{I}$ is the net collision rate at energy E. At low temperatures, the most relevant scattering mechanism is electron-electron scattering [22] and we can neglect the effect of electron-phonon scattering. Then, [10, 23]

$$\mathcal{I}(\omega,\varepsilon,E)=\mathcal{I}^{in}(\omega,\varepsilon,E)-\mathcal{I}^{out}(\omega,\varepsilon,E), \tag{6}$$

and

$$\mathcal{I}^{in}(\omega,\varepsilon,E)=(1-f(\varepsilon))(1-f(E))f(\varepsilon-\omega)f(E+\omega), \tag{7}$$
$$\mathcal{I}^{out}(\omega,\varepsilon,E)=(1-f(\varepsilon-\omega))(1-f(E+\omega))f(\varepsilon)f(E). \tag{8}$$

Electron-electron interaction is either due to direct Coulomb scattering [24, 25] or mediated by magnetic impurities [22]. Below, we concentrate on the former, but the latter would yield a similar qualitative behavior. From the calculation of the screened Coulomb interaction in the diffusive channel, it follows [24] that $\alpha=-3/2$ for a quasi-one dimensional wire and $\kappa=(\pi\sqrt{2D}\hbar^{3/2}\nu_F A_C)^{-1}$ [25, 26]. We note that Δ_C is the most relevant energy scale to describe the distribution function for different voltages V_C. It is thus useful to replace $\omega\to\omega/\Delta_C$ and $\varepsilon\to\varepsilon/\Delta_C$, in order to obtain a dimensionless equation. Multiplying Eq. (5) by $e^2\mathcal{R}_T\Omega_C\nu_F$ we obtain

$$\mathcal{N}_1(\mathcal{F}_1-f(E))-\mathcal{N}_2(f(E)-\mathcal{F}_2)= \\ =\mathcal{K}_{coll}\int d\omega d\varepsilon\omega^{-3/2}\mathcal{I}(\omega,\varepsilon,E), \tag{9}$$

where

$$\mathcal{K}_{coll}=\frac{\mathcal{R}_T}{R_C}\frac{L_C^2\kappa}{D}\sqrt{\Delta_C}=\frac{1}{\sqrt{2}}\frac{\mathcal{R}_T}{R_K}\sqrt{\frac{\Delta_C}{E_{Th}^C}}, \tag{10}$$

$R_K=h/2e^2$ and $E_{Th}^C=\hbar D/L_C^2$. In the absence of electron-electron interaction ($\mathcal{K}_{coll}=0$), Eq. (4) is recovered.

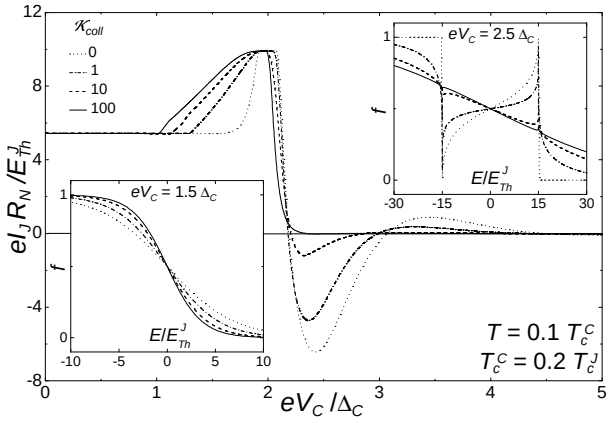

FIG. 3: Supercurrent vs V_C for various $\mathcal{K}_{coll}$ with $T = 0.1\,T_c^C$ and $T_c^C = 0.2\,T_c^J$. Insets show the distribution function at $eV_C = 1.5\Delta_C$ (left) and $eV_C = 2.5\Delta_C$ (right) calculated for the same $\mathcal{K}_{coll}$ values.

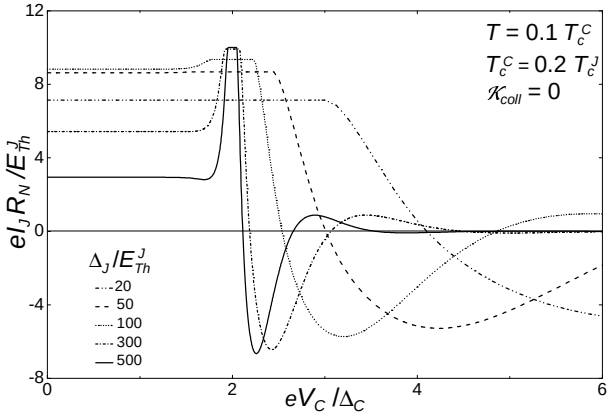

FIG. 4: Effect of different ratios Δ_J/E^J_{Th} on the observable supercurrent at $T = 0.1\,T_c^C$ and $T_c^C = 0.2\,T_c^J$. Note that the effect of the nonequilibrium distribution on the observable supercurrent is more pronounced in longer junctions.

The influence of inelastic scattering on I_J is shown in Fig. 3, which displays the critical current of a long junction at $T = 0.1\,T_c^C$ for several values of $\mathcal{K}_{coll}$. Here I_J is obtained by numerically solving Eq. (9). The effect of electron-electron interaction is to strongly suppress the π-state and to widen the peak around V_C^*. The π-transition vanishes for $\mathcal{K}_{coll} \simeq 100$, but the I_J enhancement due to quasiparticle cooling still persists in the limit of even larger inelastic scattering [27].

The disappearance of the π-state can be understood by looking at the right inset of Fig. 3 which clearly shows how a large-bias f (calculated at $eV_C = 2.5\Delta_C$) gradually relaxes from nonequilibrium towards a Fermi function upon increasing $\mathcal{K}_{coll}$. The left inset shows how a low-bias f (evaluated at $eV_C = 1.5\Delta_C$) sharpens, thus enhancing I_J, by increasing $\mathcal{K}_{coll}$. This effect follows from the fact that inelastic interactions redistribute the occupation of quasiparticle levels in the N region, thus increasing the occupation at higher energy. As a consequence, higher-energy excitations are more efficiently removed by tunneling, even for biases well below and not only around V_C^* (as in the case of $\mathcal{K}_{coll} = 0$). At the same time, supercurrent recovery at high temperature is gradually weakened upon enhancing $\mathcal{K}_{coll}$. Notably, these calculations show that a rather large amount of inelastic scattering is necessary to weaken and completely suppress the π-state. For example, using $Al/Al_2O_3/Cu$ as materials composing the SINIS line, $\mathcal{K}_{coll} = 1$ corresponds to use a fairly long control line with $L_C \simeq 4.6\ \mu$m [28].

IV. DEPENDENCE ON JUNCTION LENGTH

The choice of the superconductors S_J and S_C affects the behavior of the device through the energy scales given by the energy gaps $\Delta_{J/C}$ in these materials and their ratio with the geometric scales of the system. The role of junction length (L_J) on the transistor characteristics is displayed in Fig. 4, where the supercurrent is plotted for different ratios Δ_J/E^J_{Th} at $T = 0.1\,T_c^C$ and for $T_c^C = 0.2\,T_c^J$. Upon shortening the junction the Josephson current response to the control voltage V_C becomes wider (note that also the ratio between the characteristic energies Δ_C and E^J_{Th} changes — our model holds only for $\Delta_J \gtrsim \Delta_C$). At the same time, features like supercurrent enhancement and π-transition appear less pronounced. This suggests that large Δ_J/E^J_{Th} ratios are favorable for an efficient transistor effect, so that the $I_J(V_C)$ characteristic is forced into a narrower bias window.

V. EFFECT OF EXTRA TERMINALS

As mentioned earlier, the presence of the lateral arms influences the superconducting correlations induced in the weak link by reducing [13] the spectral supercurrent. Such an effect is shown in Fig. 5 where the equilibrium supercurrent (i.e., at $V_C = 0$) is plotted as a function of the ratio L_C/L_J. The magnitude of the supercurrent is decreased upon increasing L_C, reaching its asymptotic value at $L_C \simeq L_J$, almost independently of temperature. Note that, for each temperature, such a value is roughly one half that corresponding to the limit $L_C \to 0$. This conclusion contrasts with the case of a normal control line without tunnel barriers [9, 13] and emphasizes the relevance of the condition $L_C \ll L_J$ towards the maximization of the supercurrent in the system.

VI. PHASE DEPENDENCE

The generic sinusoidal supercurrent-phase dependence is strictly valid only in the case when the Josephson junc-

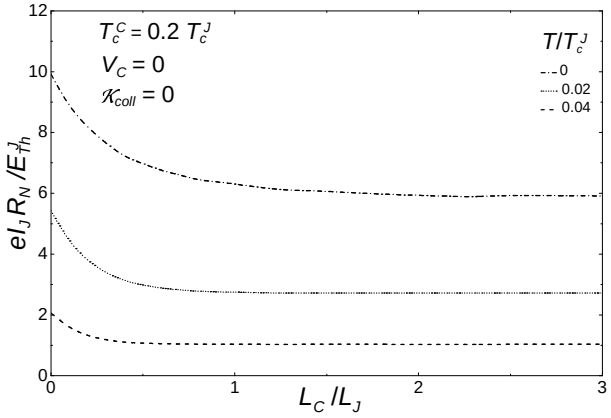

FIG. 5: Equilibrium supercurrent vs L_C/L_J at different temperatures. Note that I_J reaches its asymptotic value at $L_C \simeq L_J$, almost independently of the temperature.

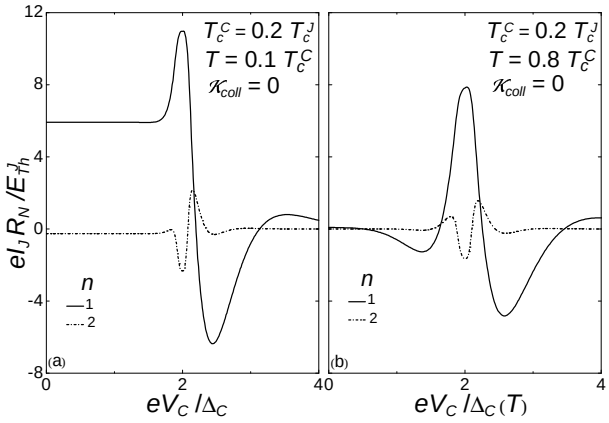

FIG. 6: (a) Voltage dependence of the amplitude of the first two harmonics of the observable supercurrent calculated at $T = 0.1\,T_c^C$ and $T_c^C = 0.2\,T_c^J$. (b) The same as in (a) calculated in the high-temperature regime ($T = 0.8\,T_c^C$).

tion is a tunnel junction. Transmission channels with high transmission probability, present in diffusive wires, tend to deform this dependence by bringing in higher harmonics. Thus, the supercurrent-phase relation is in general of the form [13]

$$I_S(\phi) = \sum_{n=1}^{\infty} I_{J,n} \sin(n\phi), \tag{11}$$

where $I_{J,n}$ are the coefficients of the Fourier sine series of $I_S(\phi)$. Loosely speaking, the higher harmonics arise from multiple passages of Cooper pairs through the junction in a single coherent process. In most cases for a diffusive junction, the $n = 1$ harmonic is dominant, and the role of the others is to slightly deform the current-phase relation, without bringing about additional nodes. However, across the π-junction transition, the first harmonic can be completely suppressed. In this case, the current-phase relation is determined by the second harmonic, and around this point, the supercurrent has a half periodicity with respect to the phase (flux in a loop). Such a $\sin(2\phi)$ phase dependence was measured in Ref. [6] in the case of normal-metallic control probes.

Figure 6 shows the voltage dependence of the two lowest harmonics at two temperatures. One can find that for most voltages, the first harmonic is dominant, but in the region(s) of the transition between the conventional and the π-states, the second becomes dominant. Moreover, one finds that, analogously to the case with normal control probes, [6, 13] the sign of the second harmonic in these regions is positive. Hence, in those values of the voltage V_C, the free energy of the junction has local minima both at $\phi = 0$ and $\phi = \pi$ [6]. Another implication of the finite value of $I_{J,2}$ around those voltages is that the critical current of the junction does not completely vanish, but it is merely no longer obtained for $\phi \approx \pi/2$.

VII. PERFORMANCE I: ROLE OF MATERIALS CHOICE

It is interesting to analyze the role of different superconductor combinations, i.e., different ratios T_c^C/T_c^J. This effect is shown in Fig. 7 where the supercurrent vs bias voltage (normalized to Δ_J/e) characteristic is displayed for different combinations of superconductors at $T = 0.02\,T_c^J$. The main effect is a shift in the I_J response along the V_C axis towards lower bias voltages upon reducing the critical temperature T_c^C. Furthermore, the shape of the characteristics appears to be virtually independent of the T_c^C value, although a small decrease of the π-transition amplitude gradually develops by decreasing the ratio T_c^C/T_c^J. Such a ratio can be chosen to move the range of relevant V_C towards lower values and thus

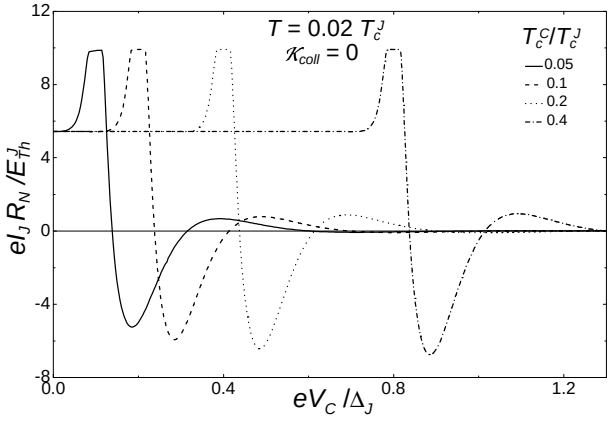

FIG. 7: Supercurrent vs V_C calculated at $T = 0.02\,T_c^J$ for different T_c^C/T_c^J ratios. The main effect of lowering T_c^C is to shift the I_J response along the V_C axis and to slightly reduce the amplitude of the π-transition.

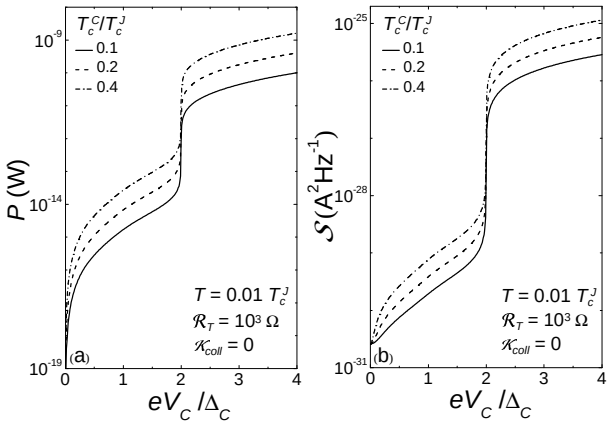

FIG. 8: (a) Power dissipated in the SINIS line vs V_C calculated for various ratios T_c^C/T_c^J and $T = 0.01 T_c^J$. (b) Noise power $\mathcal{S}$ vs V_C calculated for the same parameters as in (a). In all these calculations we set $T_c^J = 9.26$ K corresponding to Nb and $\mathcal{R}_T = 1\,k\Omega$.

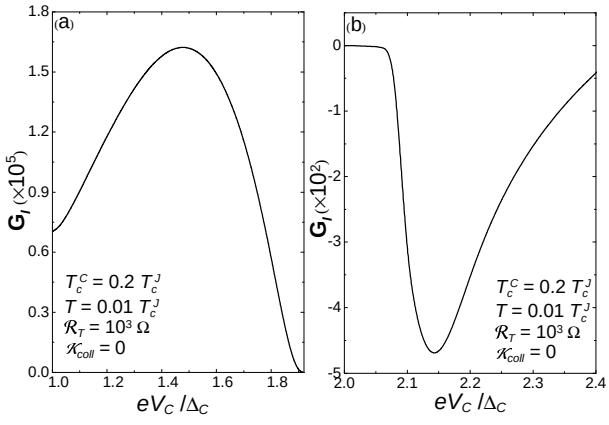

FIG. 9: Differential current gain $\mathbf{G}_I$ vs V_C for $T_c^C/T_c^J = 0.2$ and $T = 0.01\,T_c^J$: in (a) $\mathbf{G}_I$ is shown for $V_C < V_C^*$ while in (b) it is shown in the high-bias region. In these calculations we set $\mathcal{K}_{coll} = 0$ and $T_c^J = 9.26$ K (Nb).

decrease the power dissipation $P = I_C V_C$, where I_C is the control current across the SINIS channel. The function $P(V_C)$ is plotted in Fig. 8(a) for some ratios T_c^C/T_c^J at $T = 0.01\,T_c^J$, assuming $\mathcal{R}_T = 10^3\,\Omega$ and $T_c^J = 9.26$ K (corresponding to Nb). The impact of Δ_C in controlling power dissipation is easily recognized. These effects clearly point out that $\Delta_C \ll \Delta_J$ is the condition to be fulfilled in order to minimize P. In practice, the power dissipation for $eV_C > 2\Delta$ constitutes an experimental problem as this energy needs to be carried out from the reservoirs.

In a similar way the noise properties of the system are sensitive to the different T_c^C/T_c^J ratios. Assuming that the noise through one junction is essentially uncorrelated from the noise through the other, it follows that the input noise power $\mathcal{S}$ in the control line can be expressed as

$$\mathcal{S}(V_C) = \frac{1}{\mathcal{R}_T}\int_{-\infty}^{\infty} dE \mathcal{N}_1[f(E)(1-\mathcal{F}_1) + \mathcal{F}_1(1-f(E))]. \tag{12}$$

The function $\mathcal{S}(V_C)$ is shown in Fig. 8(b) for the same parameters as in Fig. 8(a). For example, for $T_c^C/T_c^J = 0.1$ (corresponding roughly to the combination Al/Nb), P obtains values of the order of a few fW and $\mathcal{S}$ of some 10^{-30} A^{2}Hz^{-1} in the cooling regime, while these values are enhanced respectively to few tens of pW and 10^{-26} A^{2}Hz^{-1} for biases around the π-transition.

VIII. PERFORMANCE II: GAIN AND SWITCHING TIME

In light of the possible use of this operational principle for device implementation, let us comment on the available gain and switching times. Input ($V_{in} = V_C$) and output ($V_{out} = I_J R_N$) voltages are of the order of Δ_C/e and E_{Th}^J/e, respectively, so that the voltage gain is $\mathbf{G}_V = V_{out}/V_{in} \approx E_{Th}^J/\Delta_C$. As $\Delta_C \to E_{Th}^J$, the device characteristics become smoother (see Sec. IV) and the control becomes less efficient, so that it is hardly possible to achieve voltage gain. On the other hand, differential current gain $\mathbf{G}_I = dI_J/dI_C$ can be very large. For $V_C > V_C^*$, a simple estimate gives

$$\mathbf{G}_I \sim (E_{Th}^J/\Delta_C)(\mathcal{R}_T/R_N), \tag{13}$$

meaning that with realistic ratios $\mathcal{R}_T/R_N$ ($\sim 10^3$), $\mathbf{G}_I$ can exceed 10^2. $\mathbf{G}_I(V_C)$ can be calculated noting that $\mathbf{G}_I = (\frac{dI_J}{dV_C})(\frac{dI_C}{dV_C})^{-1}$. In Fig. 9 we plot $\mathbf{G}_I$ for $T_c^C/T_c^J = 0.2$. This calculation reveals that $\mathbf{G}_I$ can reach huge values, with some 10^5 for $V_C < V_C^*$ [29] and several 10^2 in the opposite regime. Remarkably, gain is almost unchanged also in the presence of weak inelastic scattering (i.e., $\mathcal{K}_{coll} = 1$). The same holds for P and $\mathcal{S}$.

Operation of the Josephson junction in the *dissipative* regime makes it possible to exploit the system for power gain. Let us assume that the voltage across the Josephson junction (V_J) is fixed and that the current-voltage characteristic is nonhysteretic. According to the RSJ (resistively shunted junction) model [30] for overdamped junctions, the voltage drop across the junction at $T = 0$ reads

$$V_J = R_N\sqrt{I^2 - I_{Jc}^2}, \tag{14}$$

where I_{Jc} is the critical current and I is the total current through the Josephson junction. The differential power gain is defined as $\mathbf{G}_P = dP_{out}/dP_{in}$ where $P_{out} = V_J I$,

$P_{in} = V_C I_C$. Using Eq. (14) one obtains

$$\mathbf{G}_P = V_J \frac{dI}{d(V_C I_C)} = \frac{V_J I_{Jc}}{\sqrt{\left(\frac{V_J}{R_N}\right)^2 + I_{Jc}^2}} \frac{dI_{Jc}}{dI_C} \frac{dI_C}{d(V_C I_C)} \tag{15}$$

$$= \frac{I_{Jc}}{\sqrt{\left(\frac{V_J}{R_N}\right)^2 + I_{Jc}^2}} \frac{V_J}{V_C + I_C R_{\rm SINIS}(V_C)} \mathbf{G}_I, \tag{16}$$

where $R_{\rm SINIS} = dV_C/dI_C$ is the differential resistance of the SINIS line at the operating current I_C. Choosing $V_J = I_{JC} R_N$ we obtain

$$\mathbf{G}_P = \frac{V_J}{\sqrt{2}(V_C + I_C R_{\rm SINIS})} \mathbf{G}_I \geq \frac{V_J}{2\sqrt{2} V_C} \mathbf{G}_I. \tag{17}$$

The thermal smearing of Eq. (14) [30] will somewhat decrease $\mathbf{G}_P$, but not by orders of magnitude. A further simplification of Eq. (17) can be additionally given, recalling that $V_J \sim E_{Th}^J/e$ and $V_C \sim 2\Delta_C/e$, so that

$$\mathbf{G}_P \sim \frac{E_{Th}^J}{4\sqrt{2}\Delta_C} \mathbf{G}_I \simeq \mathbf{G}_V \mathbf{G}_I. \tag{18}$$

A straightforward estimate for the differential power gain from Eq. (18) gives $\mathbf{G}_P \sim 10^2 \div 10^3$ for $V_C < V_C^*$ and ~ 10 for $V_C > V_C^*$. This means that, in the suitable operating mode, the present structure is able to provide large power gain.

As a final issue we want to briefly address the time scales intrinsic to this mesoscopic device when it is operated in the dynamic regime. The highest operating frequency ν of the transistor is limited by the smallest energy in the system: $\nu \leq \min \frac{1}{h}\{\Delta_C, \Delta_J, E_{Th}^C, E_{Th}^J, h(\mathcal{R}_T \mathcal{C})^{-1}, he/I_C\}$ where $\mathcal{C}$ is the tunnel junction capacitance. For an optimized device, working frequencies of the order of 10^{11} Hz can be experimentally achieved in the high-voltage regime $V_C > V_C^*$. For $V_C < V_C^*$, conversely, the response is slower (of the order of some 10^8 Hz), owing to the large value of subgap resistance that becomes the speed-limiting factor due to the long discharging time through the junctions. However, this analysis relies on the fact that the relaxation time scales in the superconducting reservoirs in the control part of the structure are much shorter than the above scales. These scales depend on the geometry of the system (the real size of the reservoirs), but in practice, they may seriously limit the speed of the device unless special care is taken. We stress that the detailed prediction of the transistor dynamic response would require a separate analysis that is beyond the scope of the present paper.

IX. CONCLUSIONS

In this paper we have shown that superconductivity-induced nonequilibrium can be used to finely control the supercurrent flowing through a SNS Josephson junction. The peculiar quasiparticle energy distribution, realized in the normal island of a SINIS control line when a bias voltage is applied between the superconducting electrodes, allows us to drive the SNS junction into different transistor regimes. With increasing control voltage, we have found that the supercurrent first shows a steep enhancement, then undergoes a π-transition and finally decays to zero for larger voltages. Furthermore, we have analyzed in detail the effect of inelastic scattering within the normal island, the dependence of the supercurrent on the Josephson junction length, the effect of the presence of lateral arms on the spectral supercurrent, and the behavior of the supercurrent harmonics. Finally we have addressed the optimization of the device, both in terms of material choice and characteristic figures, such as current gain, power gain and operating frequencies. In view of these last points, we wish to point out that such a device could be successfully exploited as a first amplification stage in SQUID-based cryogenic electronics.

ACKNOWLEDGMENTS

We thank A. Anthore, M. H. Devoret, K. K. Likharev, F. Pierre, L. Roschier, A. M. Savin, and V. Semenov for helpful discussions. This work was supported in part by MIUR under the FIRB project RBNE01FSWY and by the EU (RTN-Nanoscale Dynamics).

[1] See, for example, *Theory of Nonequilibrium Superconductivity*, N.B. Kopnin (Clarendon Press, Oxford, 2001).
[2] J.J.A. Baselmans, A.F. Morpurgo, B.J. van Wees, and T.M. Klapwijk, Nature (London) **397**, 43 (1999).
[3] J.J.A. Baselmans, B.J. van Wees, and T.M. Klapwijk, Phys. Rev. B **63**, 094504 (2001).
[4] J. Huang, F. Pierre, T.T. Heikkilä, F.K. Wilhelm, and N.O. Birge, Phys. Rev. B **66**, 020507 (2002).
[5] R. Shaikhaidarov, A.F. Volkov, H. Takayanagi, V.T. Petrashov, and P. Delsing, Phys. Rev. B **62**, R14649 (2000).
[6] J.J.A. Baselmans, T.T. Heikkilä, B.J. van Wees, and T.M. Klapwijk, Phys. Rev. Lett. **89**, 207002 (2002).
[7] A. F. Volkov, Phys. Rev. Lett. **74**, 4730 (1995).
[8] F.K. Wilhelm, G. Schön, and A.D. Zaikin, Phys. Rev. Lett. **81**, 1682 (1998).
[9] S.-K. Yip, Phys. Rev. B **58**, 5803 (1998).
[10] H. Pothier, S. Guéron, N.O. Birge, D. Esteve, and M.H. Devoret, Phys. Rev. Lett. **79**, 3490 (1997).
[11] F. Giazotto, T.T. Heikkilä, F. Taddei, R. Fazio, J.P. Pekola, and F. Beltram, Phys. Rev. Lett. **92**, 137001 (2004).
[12] See W. Belzig, F.K. Wilhelm, C. Bruder, G. Schön, and

A.D. Zaikin, Superlattices Microstruct. **25**, 1251 (1999) and references therein.
[13] T.T. Heikkilä, J. Särkkä, and F.K. Wilhelm, Phys. Rev. B **66**, 184513 (2002).
[14] K.D. Usadel, Phys. Rev. Lett. **25**, 507 (1970).
[15] D.R. Heslinga, and T.M. Klapwijk, Phys. Rev. B **47**, 5157 (1993).
[16] A. Brinkman, A.A. Golubov, H. Rogalla, F.K. Wilhelm, and M.Yu. Kupriyanov, Phys. Rev. B **68**, 224 513 (2003).
[17] At low control voltages there is a region of energies where $\mathcal{N}_1 = \mathcal{N}_2 = 0$. We assume that there the (otherwise weak) coupling to phonons makes the distributions at those energies equal to the equilibrium Fermi distribution. A more detailed discussion and another type of coupling is given in Ref. 19.
[18] A similar behavior was predicted by J.J.A. Baselmans, Ph. D. thesis, University of Groningen (2002).
[19] J.P. Pekola, T.T. Heikkilä,A.M. Savin, J.T. Flyktman, F. Giazotto, and F.W.J. Hekking, Phys. Rev. Lett. **92**, 056804 (2004).
[20] M.M. Leivo, J.P. Pekola, and D.V. Averin, Appl. Phys. Lett. **68**, 1996 (1996).
[21] The interaction effects are not taken into account in the spectral supercurrent — this approximation worked fine in Refs. 3, 4.
[22] A. Anthore, F. Pierre, H. Pothier, and D. Esteve, Phys. Rev. Lett. **90**, 076806 (2003).
[23] K.E. Nagaev, Phys. Rev. B **52**, 4740 (1995).
[24] B.L. Altshuler and A.G. Aronov, Zh. Eksp. Teor. Fiz. **75**, 1610 (1978) [Sov. Phys. JETP **48**, 812 (1978)].
[25] A. Kamenev and A. Andreev, Phys. Rev. B **60**, 2218 (1999).
[26] B. Huard, A. Anthore, F. Pierre, H. Pothier, N.O. Birge, D. Esteve, preprint cond-mat/0404208.
[27] F. Giazotto, F. Taddei, T.T. Heikkilä, R. Fazio, and F. Beltram, Appl. Phys. Lett. **83**, 2877 (2003).
[28] This is straightforward assuming as typical parameters $\mathcal{R}_T = 10^3\ \Omega$, $D = 0.02\ \mathrm{m}^2/\mathrm{s}$ and $\Delta_C = 200\ \mu\mathrm{eV}$.
[29] In this calculation we chose to include depairing by a phenomenological, but realistic parameter $\Gamma = 10^{-4}\Delta_C$ [19]. Its omission would lead to extremely high values of $\mathbf{G}_I$. For $V_C \ll V_C^*$ and low temperature, Γ determines the differential resistance $R_{SINIS} \approx \mathcal{R}_T\Delta_C/\Gamma$ of the SINIS line. Qualitatively, the large $\mathbf{G}_I$ stems partially from the fact $R_{SINIS} \gg R_N$.
[30] V. Ambegaokar and B.I. Halperin, Phys. Rev. Lett. **22**, 1364 (1969).